J. Bangladesh Acad. Sci. 50(2); 259–268: June 2026 DOI: https://doi.org/10.3329/jbas.v50i2.90657

Journal of Bangladesh Academy of Sciences

Journal homepage: http://www.bas.org.bd/publications/jbas.html

Research Article

Synthesis and structure of diiron propane-1,3-dithiolate complex with $AsPh_3$ ligand: site selectivity of the $AsPh_3$ ligand

Md. Imran Hossain, Muhammad Abdul Quader, Nikhil Chandra Bhoumik[1,2]
Md. Manzurul Karim, and Shafikul Islam[*]
Department of Chemistry, Jahangirnagar University, Savar, Dhaka 1342, Bangladesh

ARTICLE INFO

Article History

Received: 01 March 2026
Revised: 04 May 2026
Accepted: 12 May 2026

Keywords: Diiron, Propane-1,3-dithiolate, $AsPh_3$ ligand, Crystal structure, Site selectivity, X-ray crystallography, DFT study.

ABSTRACT

This article reports the synthesis, structure, and site selectivity of the $AsPh_3$ ligands of two Fe_2 propane-1,3-dithiolate (PDT) complexes with the $AsPh_3$ ligand. The reaction of $Fe_2(CO)_6$(μ-PDT) **1** with 1.0 equivalent $AsPh_3$ at ambient temperature in the presence of Me_3NO resulted in a new diiron complex, $Fe_2(CO)_5(AsPh_3)$(μ-PDT) **2**, as red crystals (63%). The reaction of **1** with 5.0 equivalents of $AsPh_3$ under identical conditions gave **2** in 58% yield and $Fe_2(CO)_4(AsPh_3)_2$(μ-PDT) **3** in low yield (11%) as red crystals. The Me_3NO-assisted reaction of **2** with five equivalents of $AsPh_3$ gave **3** in moderate yields (42%). Both complexes contain two fused six-membered metallaheterocycles defined by Fe(S–C–C–C–S), one of them has a chair conformation, and the other attains in a boat conformation. The bulky $AsPh_3$ ligand selectively coordinated the Fe atoms to the apical site, which is sterically less crowded, as ascertained by the crystal structure. The DFT-optimized geometry of **2** was similar to its X-ray structure, and the simulated structure parameters were in good agreement with the experimental values. The optimized geometry of **2** was more stable than its isomeric model **4**, where the $AsPh_3$ ligand occupies the basal coordination site, by 1.31 kcalmol^{-1}. The HOMO and LUMO of **2** were more stable than those of model **4**. The calculated Wiberg bond indices (WBI) values for the Fe–Fe and Fe–As bonds in **2** are higher than those for the structural model **4**.

Introduction

Diiron PDT complex, $Fe_2(CO)_6$(μ-PDT) **1**, is a structural mimic of the of [FeFe]-hydrogenase cofactor (Li et al., 2005; Peters et al., 1998; Nicolet et al., 1999). This compound can be prepared by the substitution reaction of $BrCH_2CH_2CH_2Br$ with $[(\mu\text{-}S)_2Fe_2(CO)_6]^{2-}$ (Seyferth et al., 1980; Seyferth et al., 1982) or by the degradative oxidation of $Fe_3(CO)_{12}$ with PDTH (PDTH = propane-1,3-dithiol) (Seyferth et al., 1987). However, **1** is a notable precursor for FeFe hydrogenase biomimics because it undergoes CO displacement reactions even under mild conditions. Considering this background, myriad carbonyl-substituted derivatives of diiron PDT complex having the general formula $Fe_2(CO)_{6-n}L_n(\mu\text{-PDT})L_n$, where n = 1 and 2; L is the neutral ligands like phosphines (Li et al., 2005; Yin et al., 2011; Zhao et al., 2001; Zhao et al., 2002), diphosphines (Gao et. al., 2007; Liu et al.,2010; Adam et al., 2007; Ezzaher et al., 2007; Rohman et al., 2020;

[*]Corresponding author:<chem.shafik@juniv.edu>
[1] *Wazed Miah Science Research Center, Jahangirnagar University Savar, Dhaka 1342, Bangladesh*
[2]*Department of Chemistry, University of Nevada Reno, NV 89557, USA*

Rohman et al., 2022), stibines (Islam et al., 2022), and anionic ligands such as cyanide (Cloirec et al., 1999) have been reported. The bulky substituents in these complexes were in the apical position, suggesting that this position is sterically more favorable than the basal position.

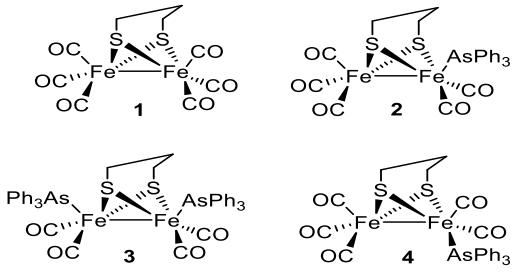

Scheme 1. Structure of the complexes described in this article.

Although most of the published articles focused on the structure and biomimetic properties of the diiron PDT-based complexes, none of them explained the site selectivity of the bulky substituents like XAr_3 (X = P, As, Sb, and Ar = aryl groups). If the site-selectivity of the voluminous substituents were properly explained, it would be insightful to clearly study the biomimetic properties. Within this context, we synthesized two diiron-PDT complexes with $AsPh_3$ ligands. The X-ray crystal structure of them showed that the $AsPh_3$ ligand, like the reported analogs, was in the apical position. We subsequently performed DFT optimization of **2** and its isomeric structural model **4** (where the $AsPh_3$ is in the basal position), and found that **2** was more stable than **4** by 1.31 kcalmol^{-1}. This value is too small to explain the site selectivity of the $AsPh_3$ ligand, however insightful. We subsequently explain the bonding interaction using natural bond orbital (NBO) and frontier molecular orbital (FMO) analyses. The synthesis, structure, and site selectivity of the $AsPh_3$ ligand of **2** and **3** are discussed herein.

Experimental

General

All chemical conversions were carried out under a dry N_2 atmosphere. Solvents were decontaminated by distillation from suitable dehydrating agents and stored in a nitrogen atmosphere prior to use. Separation of products was executed by preparative thin layer chromatography (PTLC) on silica gel (type-60 HF254, Merck, Germany). Elemental analyses were performed on the Elementar Vario EL Cube instrument. A Shimadzu IR Prestige-21 FTIR spectrophotometer gave the infrared spectra of the complexes. NMR spectra were obtained from a Bruker Avance III HD 400 MHz spectrometer. The precursor compound, **1**, was prepared according to the literature procedure (Seyferth et al., 1987). $AsPh_3$ ligand, from Aldrich Chemical Company, was used without purification.

Reaction of 1 with $AsPh_3$ in a 1:1 molar ratio

To a MeCN solution (15 mL) of 1 (100.0 mg, 0.259 mmol) and $AsPh_3$ (82.1 mg, 0.268 mmol, 1.03 *eq*) in a three-necked round bottom flask was added drop-wise a solution (15 mL) of Me_3NO (30.0 mg, 0.399 mmol, 1.54 *eq*, dissolved in the same solvent) for a period of 30 min, and the reaction mixture was stirred for an additional 20 min. The solvent was vaporized at low pressure, and the solid was chromatographed by silica gel TLC. Eluting with cyclohexane/CH_2Cl_2 (4:1, v/v) yielded a major band, which afforded **2** (108.4 mg, 63%) as red crystals from CH_2Cl_2/*n*-hexane mixture at 20 ^oC. Another pencil-thin band was too insufficient to characterize and hence discarded. Analytical and spectroscopic data for **2**: Anal. Calcd. for $C_{26}H_{21}AsFe_2O_5S_2$: C, 47.02; H, 3.19%. Found: C, 47.11; H, 3.26%. IR (υ_{CO}; in CH_2Cl_2): 2046 (s), 1985 (s, br) and 1931 (w) cm^{-1}. ^{1}H NMR (in $CDCl_3$): 7.65 (m, 6H), 7.43 (m, 9H), 1.70 (m, 4H) and 1.22 (m, 2H).

Reaction of 1 with $AsPh_3$ in a 1:5 molar ratio

A similar reaction with five equivalents of $AsPh_3$ yielded **2** (58%) and **3** (11%) as red crystals from CH_2Cl_2/*n*-hexane mixture. Analytical and spectroscopic data for **3**: Anal. Calcd. for $C_{43}H_{36}As_2Fe_2O_4S_2$: C, 54.80; H, 3.85%. Found: C, 54.89; H, 3.91%. IR (υ_{CO}; in CH_2Cl_2): 1998 (s), 1954 (m) and 1933 (s) cm^{-1}. ^{1}H NMR (in $CDCl_3$): 7.83 (m, 12H), 7.72 (m, 18H), 1.68 (m, 4H) and 1.06 (m, 2H).

Reaction of 2 with $AsPh_3$ in a 1:5 molar ratio

The reaction of **2** with five equivalents of $AsPh_3$ under identical conditions gave **3** (42%) as red crystals from CH_2Cl_2/*n*-hexane mixture.

X-ray crystallography

Crystals of **2** and **3** were obtained from the CH_2Cl_2 solution layered with *n*-hexane. A suitable crystal was selected and mounted on a Bruker APEX3 microsource diffractometer using a Nylon loop and Paratone oil. The crystal was kept at 202.0 K and 210.0 K for **2** and **3**, respectively, during data collection using Mo-Kα radiation (λ = 0.71073). Data reduction and integration were executed with the SAINT+ program (Bruker, 2015), and absorption corrections were done using the program SADABS (Bruker, 2014). The structure was solved with the ShelXS (Sheldrick, 2008) structure solution program by direct methods and refined by full-matrix least-squares based on F2 using ShelXL (Sheldrick, 2015) within the Olex2 (Dolomanov et al., 2009) graphical user interface. All atoms (except hydrogen) were refined anisotropically, and the hydrogen atoms were included using a riding model. Appurtenant crystallographic parameters are collected in Table 1.

Table 1. Crystal data and structure refinement for 2 and 3.

Parameters	**2**	**3**
Empirical formula	$C_{26}H_{21}AsFe_2O_5S_2$	$C_{43}H_{36}As_2Fe_2O_4S_2$
Formula weight	664.17	942.38
Temperature/K	202.0	210.0
Crystal system	monoclinic	triclinic
Space group	$P2_1/c$	P-1
a/Å	9.250(3)	9.299(3)
b/Å	17.263(6)	13.646(4)
c/Å	16.783(6)	16.743(5)
α/°	90	78.261(16)
β/°	101.741(12)	89.698(11)
γ/°	90	71.252(12)
Volume/Å^3	2623.9(16)	1965.5(11)
Z	4	2
ρ_{calc}g/cm^3	1.681	1.592
μ/mm^{-1}	2.552	2.557
F(000)	1336.0	952.0
Crystal size/mm^3	0.155 × 0.115 × 0.033	0.225 × 0.088 × 0.032
Radiation	MoKα (λ = 0.71073)	MoKα (λ = 0.71073)
2*Θ* range for data collection/°	4.72 to 54.4	4.476 to 54.646
Index ranges	–11 ≤ h ≤ 11 –22 ≤ k ≤ 22 –21 ≤ l ≤ 21	–11 ≤ h ≤ 11 –17 ≤ k ≤ 17 –21 ≤ l ≤ 21
Reflections collected	37584	61849
Independent reflections	5834 [R_{int} = 0.0561 R_{sigma} = 0.0438]	8777 [R_{int} = 0.0818 R_{sigma} = 0.0486]
Data/restraints/parameters	5834/0/326	8777/0/479
Goodness-of-fit on F^2	1.009	1.053
Final *R* indexes [*I*>=2*σ* (*I*)]	R_1 = 0.0319 wR_2 = 0.0591	R_1 = 0.0529 wR_2 = 0.1380
Final *R* indexes [all data]	R_1 = 0.0543 wR_2 = 0.0663	R_1 = 0.0758 wR_2 = 0.1580
Largest diff. peak/hole / e Å^{-3}	0.62/-0.37	1.61/-1.44

DFT study

The computational simulation was executed using the Gaussian 16 program (Gaussian, 2019). Initial coordinates of **2** were generated from the CIF and optimized using gradient corrected density functional theory (DFT) method with a combination of Becke's three-parameter exchange functional (Becke, 1993) and Lee-Yang-Parr correlation functional (Lee et al., 1988). The iron and arsenic atoms were represented by Los Alamos National Laboratory (LANL) effective core potential (ECP) and a LanL2DZ basis set (Wadt and Hay, 1985), while a 6-31G(d) basis set was employed for the remaining elements (Gaussian 16, Revision C.01). The initial geometry of **4** was created using the optimized geometry of **2** and changing the position of the $AsPh_3$ ligand to the basal position, and it was optimized by identical methods and basis set. The relative stability of **2** and **4** was determined by the energy difference between them. No imaginary frequency was found in the optimized geometry of **2** and **4**, as expected. This suggested that the optimized geometries of **2** and **4** are the true minima of their potential energy surfaces. The NBO analysis was done to calculate the WBI indices of **2** and **4**.

Results and Discussion

Syntheses and spectroscopic characterization of 2 and 3

The reaction of 1 with $AsPh_3$ (1.0 eq) in MeCN at rt facilitated with Me_3NO resulted in the isolation of 2, as red crystals (63%). The reaction of 1 with 2.0 equivalents of $AsPh_3$ under identical conditions resulted in **2** and a trace product which was insufficient to characterize but assumed to be **3**. We subsequently carried out the reaction with 5.0 equivalents of $AsPh_3$, keeping other parameters identical, and isolated **2** (major, 58%) and **3** (minor, 11%) as red crystals. The Me_3NO-initiated reaction of **2** with $AsPh_3$ (5.0 eq) also gave **3** in 42% yield (Scheme 2). Compound 3 was a minor isomer even at a high Fe_2-PDT to $AsPh_3$ ratio because of two bulky $AsPh_3$ ligands, which made its formation thermodynamically unfavorable.

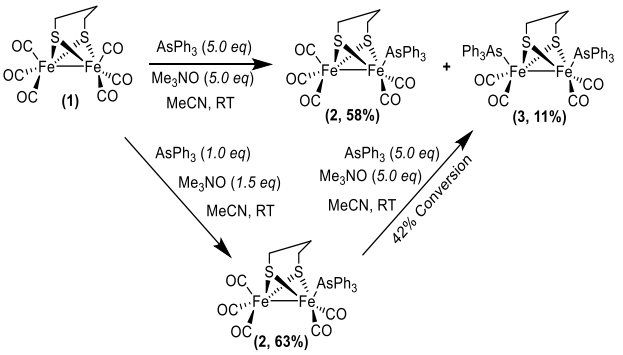

Scheme 2. Synthesis of 2 and 3.

Both **2** and **3** showed satisfactory results in their elemental analyses, supporting their structures. The solution (CH_2Cl_2) IR spectrum of **2** showed bands at 2046 (s), 1985 (s, br), and 1931 (w) cm^{-1} for CO stretch. The pattern of the IR spectrum is very similar to the reported $SbPh_3$ analog (Islam et al., 2022) and the $AsPh_3$ derivative of diiron ethane-1,2-dithiolate (EDT) complex (Ghosh et al., 2019). The ligation of one $AsPh_3$ to **1** resulted in a notable change in the pattern and shift of the absorption bands to the lower wave number. This is due to the stronger electron-donation capability of $AsPh_3$ than that of the carbonyl groups, which results in a stronger electron back donation from metal to anti-bonding MO of the CO ligands. The ^1H NMR spectrum of **2** displayed two discrete multiplets at 1.70 and 1.22 ppm with an intensity ratio of 2:1 for the $SCH_2CH_2CH_2S$ moiety, and two more multiplets at 7.65 and 7.43 ppm integrated to 6H and 9H, respectively, for the phenyl-protons. The CO stretching region of the IR spectrum of **3** showed bands at 1998 (s), 1954 (m), and 1933 (s) cm^{-1}. This pattern is nearly like that of the reported $SbPh_3$ analog (Islam et al., 2022). The PMR spectrum of **3** showed two discrete multiplets at 1.68 and 1.06 ppm integrating to 4H and 2H, respectively, in the aliphatic region, while its aromatic region showed two more multiplets at 7.83 and 7.72 ppm for 12H and 18H, respectively.

X-ray crystallography

The solid-state structures of **2** and **3** are shown in Fig. 1 and Fig. 2, respectively. Crystal data, data collection methods, and structure refinement parameters for **2** and **3** are shown in Table 1. Selected bond distances of **2** and

3 are compared with previously reported complexes in Table 2.

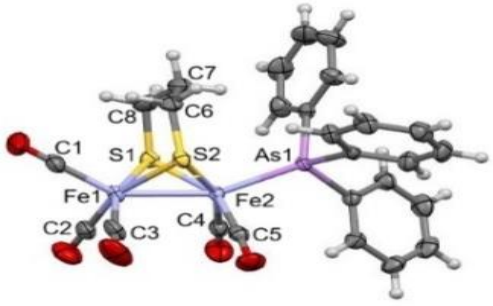

Fig. 1. Solid-state structure of 2. The atomic displacement ellipsoids are shown at the 50% probability.

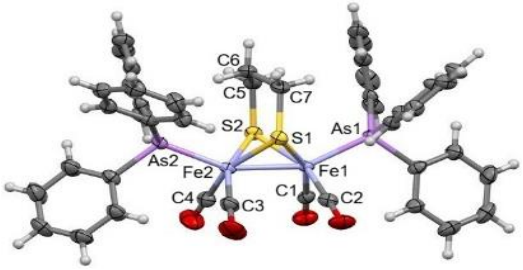

Fig. 2. Solid-state structure of 3. The atomic displacement ellipsoids are shown at the 50% probability.

Compounds **2** and **3** have a diiron framework with five and four terminal carbonyl groups, respectively, one bridging PDT ligand, and one and two apical $AsPh_3$ ligands. The core Fe_2S_2 moiety of both complexes achieves a butterfly-like shape as observed in previously reported complexes (Li et al., 2005; Zhao et al., 2001; Zhao et al., 2002; Gloaguen et al., 2001; Hasan et al., 2001; Mejia-Rodriguez et al., 2004; Ott et al., 2004; Lawrence et al., 2002; Nehring and Heinekey, 2003), and each iron atom achieves a distorted octahedral geometry. Both complexes contain two six-membered metallacycles formed by Fe/S/C/C/C/S atoms, which are joined together by sharing a common PDT ligand. Among them, one of which has a chair conformation, and the other is necessarily in a boat conformation. Substitution of CO by $AsPh_3$ ligands, like the PPh_3 (Li et al., 2005; Yin et al., 2011) and $SbPh_3$ (Islam et al., 2022), resulted in the shortening of the Fe–Fe bond lengths as compared to that of **1** (Lyon et al., 1999). However, the Fe−Fe bond distances of **2** and **3** are within the range of the reported XPh_3 derivatives of diiron-EDT (X = P, As, and Sb) (Ghosh et al., 2019) and diiron-PDT (X = P and Sb) (Li et al., 2005; Islam et al., 2022) complexes (Table 2). The mean Fe−C bond distances in **2** and **3** are *ca.* 1.758(3) Å and 1.762(4) Å, respectively, which are lower than the mean Fe−C bond length (1.800(3) Å) of **1** (Lyon et al., 1999). In both complexes, the $AsPh_3$ ligands selectively occupy the apical coordination sites. Computational study revealed that complex **2** is 1.31 $kcalmol^{-1}$ more stable than its isomeric model **4**, where the $AsPh_3$ is in the basal position. This is further justified by frontier molecular orbital analysis and electronic structure calculations (*vide infra*).

The Fe−Fe bond length in **3** is slightly lower than that in **2**, and moving from **1** to **3**, there is a gradual shortening of the Fe−Fe bond. This phenomenon is explained by the stronger electron-donating capacity of $AsPh_3$ than that of CO, and hence, there is an increase in the electron density in the Fe−Fe bond. The Fe−Fe bond in **3** is slightly shorter than the PPh_3 analog (Yin et al., 2011), but slightly longer than the $SbPh_3$ counterpart (Islam et al., 2022). A similar trend is observed for XPh_3 (X = P, As, Sb) ligated ethane-1,2-dithiolate complexes (Table 2) (Ghosh et al., 2019). Therefore, the electron-donating capacity of XPh_3 ligands to the diiron-dithiolate complexes is assumed to follow the order of OC < PPh_3 < $AsPh_3$ < $SbPh_3$.

DFT study

The optimized geometry—The structural parameters and stability of **2** were confirmed using DFT study with the Gaussian 16 program (Gaussian, 2019). Another isomeric structural model, **4,** in which $AsPh_3$ is in the basal position, was optimized using identical level of theory. However, complex **2** was 1.31 kcal/mol more stable than model **4**, suggesting that the bulky $AsPh_3$ selectively occupies the apical coordination site, which is energetically favorable (Fig. 3). Based on the crystal structures of **2** and **3**, and DFT optimized geometry of **2** and **4**, it was apparently assumed that the apical coordination sites of them were sterically less crowded. This information would be insightful in the development of new diiron dithiolate-based complexes with XAr_3 (X = P, As, Sb; Ar = aryl groups) type ligands.

Table 2. Selected bond distances of 2, 3, and some related complexes.

Complex	d_{Fe-Fe} (Å)	d_{Fe-X} (Å) (X = P, As, Sb)	Av. d_{Fe-C} (Å)[a]	Av. d_{Fe-C} (Å)[b]	Av. d_{C-O} (Å)[a]	Av. d_{C-O} (Å)[b]	Ref.
$Fe_2(CO)_5(PPh_3)(\mu$-edt)	2.5107(4)	2.2382(6)	1.769(2)	1.790(2)	1.150(3)	1.144(3)	(Ghosh et al., 2019)
$Fe_2(CO)_5$ $(AsPh_3)(\mu$-edt)	2.5010(8)	2.3316(7)	1.774(4)	1.788(5)	1.140(4)	1.143(5)	(Ghosh et al., 2019)
$Fe_2(CO)_5(SbPh_3)(\mu$-edt)	2.5034(4)	2.4727(3)	1.769(2)	1.797(3)	1.150(3)	1.136(3)	(Ghosh et al., 2019)
$Fe_2(CO)_6(\mu$-pdt)	2.5103(11)	-	-	1.800(3)	-	1.136(4)	(Lyon et al., 1999)
$Fe_2(CO)_5(PPh_3)(\mu$-pdt)	2.5247(6)	2.2566(9)	1.758(4)	1.785(4)	1.142(5)	1.141(5)	(Li et al., 2005)
$Fe_2(CO)_5(SbPh_3)(\mu$-pdt)	2.5067 (8)	2.4873 (8)	1.765(2)	1.790(2)	1.144(2)	1.136(3)	(Islam et al., 2022)
2	2.5066(8) [2.47533]	2.3410(8) [2.42318]	1.758(3) [1.77599]	1.786(3) [1.78850]	1.143(3) [1.15459]	1.135(3) [1.15182]	(This study)
$Fe_2(CO)_4(PPh_3)_2(\mu$-edt)	2.5074(5)	2.2427(6) 2.2264(6)	1.764(2)	-	1.154(2)	-	(Ghosh et al., 2019)
$Fe_2(CO)_4(AsPh_3)_2(\mu$-edt)	2.4858(5)	2.3214(4) 2.3362(5)	1.768(3)	-	1.149(3)	-	(Ghosh et al., 2019)
$Fe_2(CO)_4(SbPh_3)_2(\mu$-edt)	2.4741(4)	2.4722(4) 2.4688(3)	1.769(2)	-	1.146(2)	-	(Ghosh et al., 2019)
$Fe_2(CO)_4(PPh_3)_2(\mu$-pdt)	2.5167(16)	2.237(2) 2.230(2)	1.740(8)	-	1.169(8)	-	(Yin et al., 2011)
$Fe_2(CO)_4(SbPh_3)_2(\mu$-pdt)	2.4786 (9)	2.4726(9) 2.4626(9)	1.764(3)	-	1.144(4)	-	(Islam et al., 2022)
3	2.4907(11)	2.3351(9) 2.3296(10)	1.762(4)	-	1.146(4)	-	(This study)

[a]Defined for substituted Fe core; [b]Defined for unsubstituted Fe core. Simulated structural parameters for **2** are in square brackets.

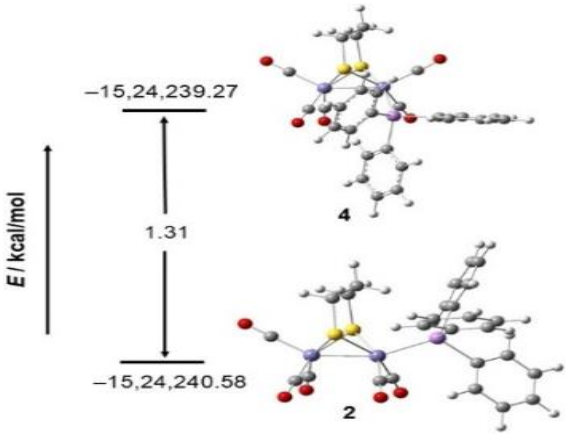

Fig. 3. Optimized geometries of 2 and the structural model 4 at B3LYP/6-31G*/LanL2DZ (for Fe and As) level of theory. Color code: gray, C; light gray, H; red, O; yellow, S; pink, As; light blue, Fe.

*The electronic structure of **2** and **4**—* The highest occupied molecular orbital (HOMO) and the lowest unoccupied molecular orbital (LUMO) for **2** and **4**, and their energies are compared in Fig. 4. Stronger Fe–As interaction is observed in **2** than that in **4**, and **2** has stabilized HOMO (by 0.1 eV) and LUMO (by 0.09 eV) than the structural model **4**. This suggests the apical position is electronically more favorable for bonding with the $AsPh_3$ ligand than the basal site. However, the HOMO-LUMO energy gap for **2** and **4** is almost equal.

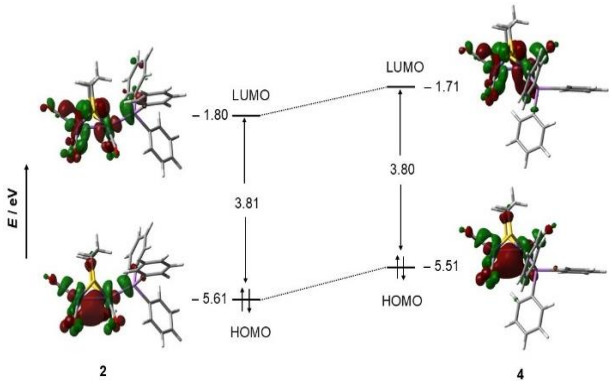

Fig. 4. Frontier molecular orbital analysis of 2 and 4.

For both **2** and **4**, the HOMO is a bonding-type MO, whereas the LUMO is an antibonding-type MO. However, the HOMO and LUMO of **2** display an antibonding type interaction between an Fe atom and the As atom, which results in higher electron density between the two iron atoms. Such an interaction is negligible in model **4** (Fig. 4). To quantify this, NBO analysis was performed for **2** and **4**. The calculated WBI values for the Fe–Fe and Fe–As bonds are 0.5026 and 0.7285 for **2**, respectively. In contrast, the WBI values for Fe–Fe and Fe–As bonds are 0.4640 and 0.7228 for **4**, respectively. Therefore, the apical site selectivity of the $AsPh_3$ ligand in the diiron dithiolate system is controlled by the steric factor (as observed from the structure) and the electronic factor.

Conclusion

Two diiron-PDT complexes with apical $AsPh_3$ ligands were synthesized and structurally characterized. For both complexes, the bulky $AsPh_3$ ligand coordinated to the iron atoms at the apical coordination site as observed in their X-ray crystal structures. This is expected as the apical site is sterically less crowded than the basal positions. The apical site selectivity of the $AsPh_3$ ligand in the Fe_2-PDT system was justified by the DFT study, as the $AsPh_3$ group of **2** in the apical position was 1.31 $kcalmol^{-1}$ more stable than model **4**, where the $AsPh_3$ ligand was in the basal position. Additionally, frontier molecular orbital analysis and electronic structure calculations based on NBO analysis indicated that the apical coordination site is electronically more favorable than the basal positions. Therefore, the apical site selectivity of the $AsPh_3$ ligand in the diiron dithiolate complexes is controlled by the steric and electronic factors. The results of this article are insightful for the development of future diiron dithiolate-based complexes, and to clarify their reactivity.

Supporting Information

CCDC 2074724 and CCDC 2074725 refer to the crystallographic data for **2** and **3**. Copy of this data can be obtained free of charge through the link, https://www.ccdc.cam.ac.uk/conts/retrieving.html (or from Cambridge Crystallographic Data Centre, 12 Union Road, Cambridge CB2 1EZ, UK (Tel: +441223 336408; fax: +44 1223 336033; email: deposit@ccdc.cam.ac.uk)).

Acknowledgment

The authors acknowledge Jahangirnagar University for financial support and Wazed Miah Science Research Center, Jahangirnagar University, for providing analytical data, recording IR and ^1H NMR spectra, and for the single-crystal X-ray diffraction study of the complexes. SI is thankful to Professor K.-i. Sugiura of Tokyo Metropolitan University, Japan, for technological support of computational studies.

Authors contribution

MIH: Synthesis and spectroscopy study; MAQ: Synthesis and spectroscopy study; NCB: Crystallographic study; SI: Conceptualization, Computational study, Writing and reviewing manuscript; MMK: Fund acquisition, Conceptualization, Supervision.

Conflict of interest

The authors declare no competing financial interests.

References

Adam FI, Hogarth G, and Richards I. Models of the iron-only hydrogenase: Reactions of $[Fe_2(CO)_6(\mu\text{-pdt})]$ with small bite-angle diphosphines yielding bridge and chelate diphosphine complexes $[Fe_2(CO)_4(\text{diphosphine})(\mu\text{-pdt})]$. *J. Organomet. Chem.* 2007a; 692: 3957–3968.

Adam FI, Hogarth G, Richards I, and Sanchez BE. Models of the iron-only hydrogenase: Structural studies of chelating diphosphine complexes $[Fe_2(CO)_4(\mu\text{-pdt})(\kappa^2P,P'\text{-diphosphine})]$. *Dalton Trans.* 2007b; 24: 2495–2498.

Becke AD. Density-functional thermochemistry. III. The role of exact exchange. *J. Chem. Phys.* 1993; 98: 5648–5652.

Bruker SADABS-2014/5, Bruker AXS Inc. 2014, Madison, Wisconsin, USA.

Bruker SAINT (8.37A), Bruker AXS Inc. 2015, Madison, Wisconsin, USA.

Cloirec AL, Best SP, Borg S, Davies SC, Evans DJ, Hughes DL, and Pickett CJ. A di-iron dithiolate possessing structural elements of the carbonyl/cyanide sub-site of the H-centre of Fe-only hydrogenase. *Chem. Commun.* 1999; 2285–2286.

Dolomanov OV, Bourhis LJ, Gildea RJ, Howard JAK, Puschmann H. *OLEX2*: a complete structure solution, refinement and analysis program. *J. Appl. Crystallogr*. 2009; 42: 339–341.

Ezzaher S, Capon JF, Gloaguen F, Petillon FY, Schollhammer P, Talarmin J, Pichon R, and Kervarec N. Evidence for the formation of terminal hydrides by protonation of an asymmetric iron hydrogenase active site mimic. *Inorg. Chem*. 2007; 46: 3426–3428.

Gao W, Ekstrom J, Liu J, Chen C, Eriksson L, Weng L, Kermark BA, and Sun L. Binuclear iron−sulfur complexes with bidentate phosphine ligands as active site models of Fe-hydrogenase and their catalytic proton reduction. *Inorg. Chem.* 2007, 46: 1981–1991.

Gaussian 16, Revision C.01, Frisch MJ, Trucks GW, Schlegel HB, Scuseria GE, Robb MA, Cheeseman JR, Scalmani G, Barone V, Petersson GA, Nakatsuji H, Li X, Caricato M, Marenich AV, Bloino J, Janesko BG, Gomperts R, Mennucci B, Hratchian HP, Ortiz JV, Izmaylov AF, Sonnenberg JL, Williams-Young D, Ding F, Lipparini F, Egidi F, Goings J, Peng B, Petrone A, Henderson T, Ranasinghe D, Zakrzewski VG, Gao J, Rega N, Zheng G, Liang W, Hada M, Ehara M, Toyota K, Fukuda R, Hasegawa J, Ishida M, Nakajima T, Honda Y, Kitao O, Nakai H, Vreven T, Throssell K, Montgomery JA Jr, Peralta JE, Ogliaro F, Bearpark MJ, Heyd JJ, Brothers EN, Kudin KN, Staroverov VN, Keith TA, Kobayashi R, Normand J, Raghavachari K, Rendell AP, Burant JC, Iyengar SS, Tomasi J, Cossi M, Millam JM, Klene M, Adamo C, Cammi R, Ochterski JW, Martin RL, Morokuma K, Farkas O, Foresman JB, and Fox DJ, Gaussian, Inc., 2019, Wallingford CT.

Ghosh S, Rahaman A, Orton G, Gregori G, Bernat M, Kulsume U, Hollingsworth N, Holt KB, Kabir SE, and Hogarth G. Synthesis, molecular structures and electrochemical investigations of [FeFe]-hydrogenase biomimics $[Fe_2(CO)_{6-n}(EPh_3)_n(\mu\text{-edt})]$ (E = P, As, Sb; n = 1, 2). *Eur. J. Inorg. Chem.* 2019; 42: 4506–4515.

Gloaguen F, Lawrence JD, and Rauchfuss TB. Biomimetic hydrogen evolution catalyzed by an iron carbonyl thiolate. *J. Am. Chem. Soc.* 2001; 123 (38): 9476–9477.

Gloaguen F, Lawrence JD, Schmidt M, Wilson SR, and Rauchfuss TB. Synthetic and Structural Studies on $[Fe_2(SR)_2(CN)_x(CO)_{6-x}]x-$ as active site models for fe-only hydrogenases. *J. Am. Chem. Soc.* 2001, 123(50): 12518–12527.

Hasan MM, Hursthouse MB, Kabir SE, and Malik KMA. Dinuclear iron carbonyl complexes with dithiolate ligands: X-ray structures of $[Fe_2(CO)_6\{\mu\text{-SCCHCHC}(CH_3)\text{CHCS}\}]$ and $[Fe_2(CO)_5\{\mu\text{-SCCHCHC}(CH_3)\text{CHCS}\}(PPh_3)]$. *Polyhedron,* 2001; 20: 97–101.

Islam S, Hossain MI, Karim MM, and Bhoumik NC. Carbonyl displacement reaction in diiron propane-dithiolate complex by triphenylstibine: Crystal structure of $[Fe_2(CO)_{6-n}(SbPh_3)_n(\mu\text{-}S_2C_3H_6)]$ (n = 1 and 2). *J. Chem. Crystallogr.* 2022; 52(1): 17–24.

Lawrence JD, Rauchfuss TB, and Wilson SR. New class of diiron dithiolates related to the Fe-only hydrogenase active site: Synthesis and characterization of $[Fe_2(SR)_2(CNMe)_7]2+$. *Inorg. Chem.* 2002; 41: 6193–6195.

Lee C, Yang W, and Parr RG. Development of the Colle-Salvetti correlation-energy formula into a functional of the electron density. *Phys. Rev. B. Condens. Matter*. 1988; 37(2): 785–789.

Li P, Wang M, He C, Li G, Liu X, Chen C, Åkermark B, and Sun L. Influence of tertiary phosphanes on the coordination configurations and electrochemical properties of iron hydrogenase model complexes: crystal structures of $[(\mu\text{-}S_2C_3H_6)Fe_2(CO)_{6-n}L_n]$ (L = PMe_2Ph, $n = 1, 2$; PPh_3, $P(OEt)_3$, $n = 1$). *Eur. J. Inorg. Chem.* 2005; 2005(12): 2506–2513.

Liu XF and Yin BS. Synthesis and structural characterization of a diiron propanedithiolate complex $[(\mu\text{-PDT})Fe_2(CO)_5]_2[(\eta^5\text{-}Ph_2PC_5H_4)_2Fe]$ containing a bidentate phosphine ligand 1,1′-bis(diphenylphosphino)ferrocene. *J. Coord. Chem.* 2010; 63: 4061.

Lyon EJ, Georgakaki IP, Reibenspies JH, and Darensbourg MY. Carbon monoxide and cyanide ligands in a classical organometallic complex model for Fe-only hydrogenase. *Angew. Chem. Int. Ed.* 1999; 38(21): 3178–3180.

Mejia-Rodriguez R, Chong D, Reibenspies JH, Soriaga MP, and Darensbourg MY. The hydrophilic phosphatriazaadamantane ligand in the development of H_2 production electrocatalysts: Iron hydrogenase model complexes. *J. Am. Chem. Soc.* 2004; 126(38): 12004–12014.

Nehring JL and Heinekey DV. Dinuclear iron isonitrile complexes: models for the iron hydrogenase active site. *Inorg. Chem.* 2003; 42(14): 4288–4292.

Nicolet Y, Piras C, Legrand, Hatchikian CE, and Fontecilla-Camps. Desulfovibrio desulfuricans iron hydrogenase: the structure shows unusual coordination to an active site Fe binuclear center. *Struc.* 1999; 7(1): 13–23.

Ott S, Borgström M, Kritikos M, Lomoth R, Bergquist J, Åkermark B, Hammarström L, and Sun L. Model of the iron hydrogenase active site covalently linked to a ruthenium photosensitizer: Synthesis and photophysical properties. *Inorg. Chem.* 2004; 43(15): 4683–4692.

Peters JW, Lanzilotta WN, Lemon B, and Seefeldt LC. X-ray crystal structure of the Fe-only hydrogenase (CpI) from Clostridium pasteurianum to 1.8 angstrom resolution. *Sci.* 1998; 282(5395): 1853–1858.

Rohman MM, Hossain MI, Bhoumik NC, Islam S, and Karim MM. A tetranuclear propane-1,3-dithiolate complex, $[Fe_2(CO)_5\{Ph_2P(CH_2)_3\}\{(\mu\text{-}SCH_2)_2CH_2\}]_2$, with a Bridging 1,6-Bis(diphenylphosphino)hexane Ligand. *J. Chem. Crystallogr.* 2022; 52:223–232.

Rohman MM, Rahman MA, Karim MM, Bhoumik NC, and Islam S. A diiron propane-1,3-dithiolate complex, $[Fe_2(CO)_4(\kappa^2\text{-dpbp})\{\mu\text{-}(SCH_2)_2CH_2\}]$, with a chelating dpbp [dpbp = 2,2′-bis(diphenylphosphino)- 1,1′-biphenyl] ligand. *J. Bangladesh Chem. Soc.* 2020; 32: 36–40.

Seyferth D, Henderson RS, and Song LC. Chemistry of μ-dithio-bis(tricarbonyliron), a mimic of organic disulfides. 1. Formation of di-.mu.-thiolate-bis(tricarbonyliron) dianion. *Organomet.* 1982; 1: 125–133.

Seyferth D, Henderson RS, and Song LC. The dithiobis(tricarbonyliron) dianion: Improved preparation and new chemistry. *J. Organomet. Chem.* 1980; 192: C1.

Seyferth D, Womack GB, Gallagher MK, Cowie M, Hames BW, Fackler Jr JP, and Mazany AM. Novel anionic rearrangements in

hexacarbonyldiiron complexes of chelating organosulfur ligands. *Organomet.* 1987; 6(2): 283–294.

Sheldrick GM. A Short History of SHELX. *Acta Crystallogr.* 2008; 64: 112–122.

Sheldrick GM. Crystal Structure Refinement with SHELXL. *Acta Crystallogr.* 2015; 71: 3–8.

Wadt WR and Hay PJ. *Ab initio* effective core potentials for molecular calculations. Potentials for the transition metal atoms Sc to Hg. *J. Chem. Phys.* 1985; 82: 270–283.

Wadt WR and Hay PJ. *Ab initio* effective core potentials for molecular calculations. Potentials for K to Au, including the outermost core orbitals. *J. Chem. Phys.* 1985; 82: 299–310.

Wadt WR and Hay PJ. *Ab initio* effective core potentials for molecular calculations. Potentials for main group elements Na to Bi. *J. Chem. Phys.* 1985; 82: 284–298.

Yin BS, Li TB, and Yang MS. μ-Propane-1,3-dithiolato-$\kappa^4S,S':S,S'$-bis[dicarbonyl(triphenylphosphane-κP) iron(II)](*Fe—Fe*). *Acta Crystallogr.* 2011; 67: m1502.

Zhao X, Georgakaki IP, Miller ML, Rodriguez RM, Chiang CY, and Darensbourg MY. Catalysis of H_2/D_2 scrambling and other H/D Exchange Processes by [Fe]-Hydrogenase model complexes. *Inorg. Chem.* 2002; 41(15): 3917–3928.

Zhao X, Georgakaki IP, Miller ML, Yarbrough JC, and Darensbourg MY. H/D exchange reactions in dinuclear iron thiolates as activity assay models of Fe−H_2ase. *J. Am. Chem. Soc.* 2001; 123(39): 9710–9711.